

Available online at www.sciencedirect.com**ScienceDirect**

Energy Procedia 115 (2017) 463–479

Energy

Procediawww.elsevier.com/locate/procedia

International Conference – Alternative and Renewable Energy Quest, AREQ 2017,
1–3 February 2017, Spain

Technical Evaluation of an Improved Paint Coating with NIR Pigments Designed To Reduce Thermal Discomfort Caused By Incident Solar Radiation: Application in the Caribbean Area

Carlos-Wilbert Peña Puesan^a, Joan-Lluís Zamora Mestre^{*b}

^a*LiTA Laboratori d'innovació i Tecnologia a l'Arquitectura, Universitat Politècnica de Catalunya,
Pere Serra, 1-15, 08173 Sant Cugat del Vallès, Barcelona (Catalonia) Spain*

Abstract

The main benefits of efficient façades and roofs are reductions in the energy consumption required for cooling during the summer and greater comfort for users. Traditional insulation is based on resistance (R) to conductive heat transfer between solid objects. However, about 93% of the gain or loss of heat from buildings is due to radiation of infrared energy; the remaining 7% is due to a combination of conduction and convection.

Therefore, we proposed the use of an anti-radiant façade and roof for the Caribbean area, based on improved paint coating systems for concrete block masonry (such as the traditional façade system in the Dominican Republic) and for expanded polystyrene panels (a novel façade system on the market in the Dominican Republic). The paint coating was improved by developing and applying NIR pigments whose high reflectance parameters protect the building envelope and enhance comfort in the home.

© 2017 The Authors. Published by Elsevier B.V.
Peer-review under responsibility of the organizing committee of AREQ 2017.

Keywords: reflective coatings, NIR pigments, solar radiation, the Caribbean

* Corresponding Author: Tel:+34680632387
Email Address: joan.lluis.zamora@upc.edu

1. Background

1.1. Housing in the Caribbean region of the Dominican Republic

In the coming years [1], the Dominican Republic plans to build approximately 30,000 social houses annually. This is a decisive action to reduce the current housing deficit which, according to the Human Development Office of the United Nations Development Program, is estimated to number about 1,096,000 homes in total. The rapid pace of current population growth has not allowed the government and institutions that govern the construction sector to establish adequate architectural planning and urban control to provide a low budget model as well as a suitable response to local needs and conditions. One requirement is to provide a better qualitative response to the prevailing climatic conditions in the Caribbean region, which include intense solar radiation.

1.2. Climate

The Tropic of Cancer is situated to the north of the Dominican Republic, so the main climate in this area is humid tropical savanna. This is the characteristic climate of Santo Domingo (both the Province of Santo Domingo and the National District). There are abundant rains, little temperature variation between day and night, and few seasonal variations, combined with local microclimates. This climate has a very high amount of annual solar radiation, at between 11 and 13 hours per day [2]. According to information provided by the National Meteorological Office (ONAMET), based on data from its 26 meteorological stations, the territory of the Dominican Republic has average overall annual solar radiation that ranges from 5.0 to 6.0 kWh/m², with a gradient from the east to the west of the country. The city of Santo Domingo has average annual overall solar radiation of 4.61 kWh/m² (see Figure 01).

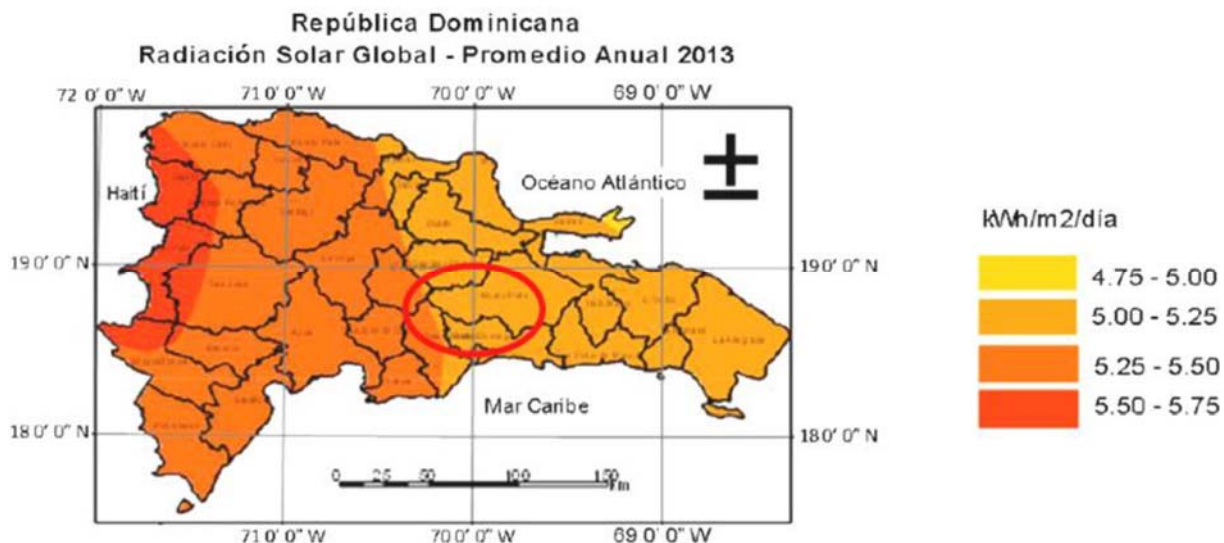


Figure 01. Overall annual average solar radiation. Source: National Meteorological Office (ONAMET)

The temperatures vary between 18°C and 25°C throughout the year and over the region, with an average of 25°C. There are cooler places like Constanza, with an average temperature of 18°C, and warmer places, such as Mao and Azua, with an average of 27°C. The coldest month is January and the warmest month is August. At higher altitudes, the temperature can drop considerably in winter, with temperatures below 10°C. The geographical distribution of temperatures in the Dominican Republic in the different months of the year is best illustrated by isothermal maps (see Figure 02).



Mes	Media de las temperaturas mínimas diarias (°C)	Media de las temperaturas máximas diarias (°C)	Precipitación total media (mm)	Media del número de días de lluvia
Ene	19.6	29.2	63	7.6
Feb	19.7	29.2	56.8	6.3
Mar	20.2	29.6	53.8	6.3
Abr	21.1	30.2	71.9	7
May	22.2	30.4	187.7	11.3
Jun	22.9	30.8	140.1	10.3
Jul	22.8	31.3	144.6	11.4
Ago	22.7	31.5	177.4	12
Sep	22.7	31.4	180.9	11.8
Oct	22.3	31.1	186.8	13
Nov	21.4	30.6	99.8	9.4
Dic	20.3	29.6	84.3	9

Figure 02: Isothermal temperatures and maximum and minimum rainfall throughout the year in the Dominican Republic. Source: National Meteorological Office (ONAMET), 2014

The wet load that the trade winds drag from the Atlantic Ocean to the northeast of the country produces what are known as orographic rains. The rains occur first in the Cordillera Septentrional, the Sierra de Yamasá and then in the Cordillera Central. The annual values of rainfall in these areas range from 1,800 to 2,500 mm, with exceptions in the karst zone of Los Haitises, where precipitation values have been recorded above 3,000 mm per year [3]. Rainfall levels are distributed over three seasons:

- Frontal season (November–April)
- Convective season (May–July)
- Cyclonic season (August–October)

The greatest rainfall is recorded during the convective and cyclonic (May–October) seasons, while drought occurs during the frontal season (November–April); in spite of the reduction in precipitation, the coolest temperatures usually occur during this period.

The trade winds from the northeast mitigate the effects of solar radiation and humidity throughout almost all of the year. The average annual wind speed is 10.1 Km/h, with a minimum of 8.8 Km/h and a maximum of 10.9 Km/h. The territory of the Dominican Republic experiences extraordinary levels of wind produced by the passage of hurricanes or tropical cyclones during the Atlantic hurricane season (01 June–30 November), as a consequence of being located in the area where most of these natural phenomena occur (the approximate average wind speed in the most unfavorable conditions is about 186.4 km/h).

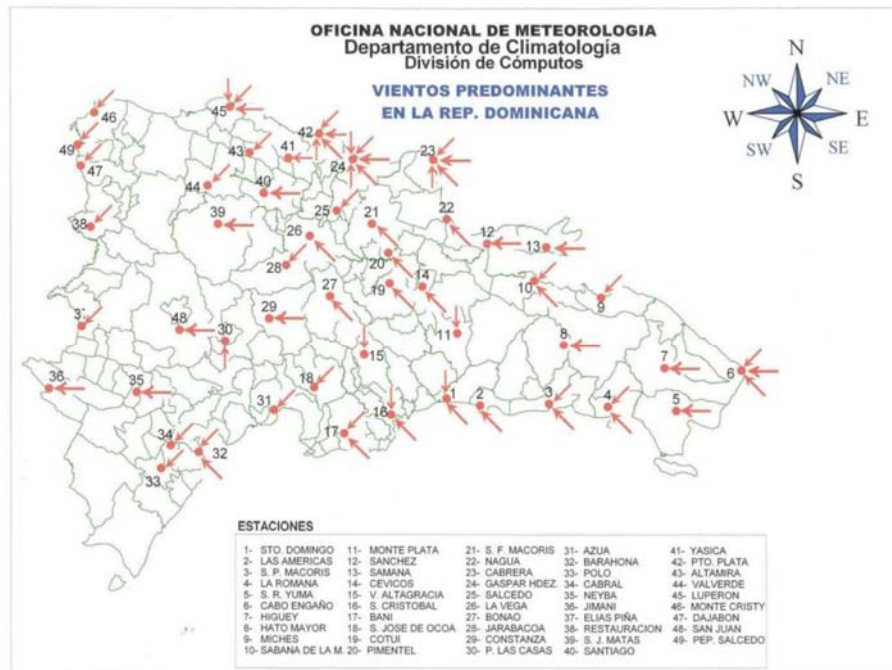


Figure 03. Direction and intensity of prevailing winds in the Dominican Republic. Source: National Meteorological Office (ONAMET)

1.3. Reflective coatings

The greatest source of heat we have in the biosphere is solar radiation, whether direct or indirect (diffuse radiation through the atmosphere). Solar radiation has a certain frequency spectrum in which the infrared fraction is notable. Infrared radiation (IR) is located just after the visible spectrum (what we popularly call light), precisely because it is beyond the range associated with the red color. This part of the spectrum covers wavelengths between 780 nanometers (nm) and 1.0 millimeters (mm), although it is usually subdivided into three categories:

- Near infrared: 780 nm to 2.5 micrometers (μm)
- Medium infrared: 2.5 μm to 50 μm
- Far infrared: 50 μm to 1mm

Infrared is the type of electromagnetic radiation that is particularly noticeable to humans through the thermal sensors of our skin. For example, we perceive near infrared when we expose ourselves directly to the rays of the sun and when we are near a fire or a high-temperature object. Medium and far infrared are emitted by any object at terrestrial temperature (approximately between -10°C and 100°C). Far infrared can be emitted by any object with a temperature above absolute zero (-273°C). Infrared radiation plays a key role in the thermal behavior of buildings. When building envelopes and particularly façades and roofs receive solar radiation, they reflect part of it whilst another part passes through glazed openings. The remaining part of the radiation is absorbed by opaque facings. The opaque surfaces are heated and in turn re-emit the radiation in all directions, contributing in part to the discomfort felt in overheated interiors (see Figure 04).

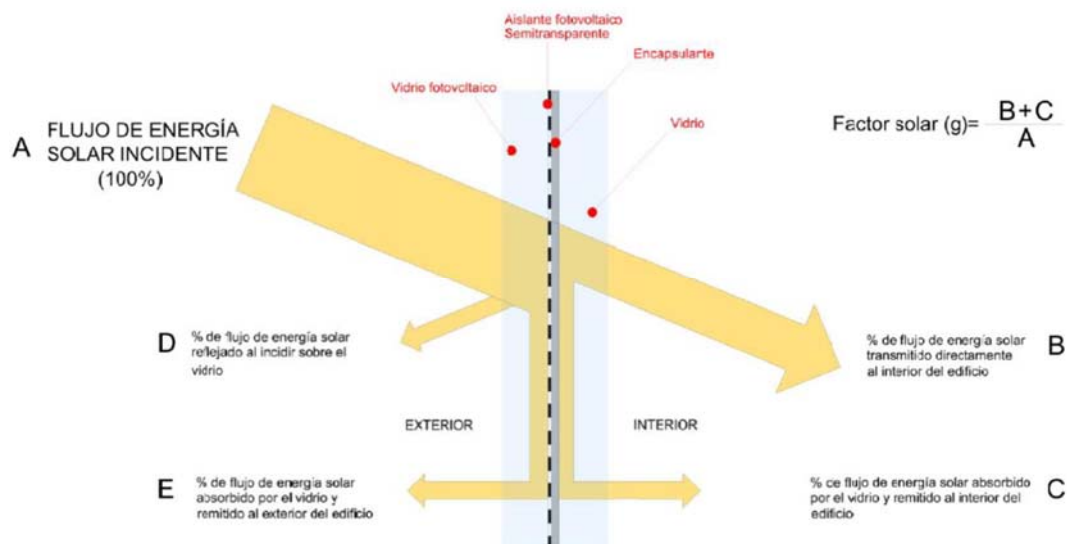


Figure 04. Percentage distribution of incident solar radiation on the vertical enclosure of a building, in this case glass.

Source: <http://www.solarinnova.net/pt/productos/fotovoltaica/modulos/bipv/vidrio-vidrio>

Numerous studies [4] support the benefits of external cladding for buildings using suitable materials that will protect the interior against the direct incidence of solar radiation in climates with high temperatures and intense solar radiation. In optics and thermodynamics, the parameter “reflectivity” represents the fraction of the incident radiation that is reflected by a surface. In general terms, reflectivity is considered a directional property, because in addition to the incident wavelength, it depends on the direction of the incident radiation and the direction of the reflected radiation. The term reflectivity is a parameter that is used to characterize thick reflective coatings, unlike the particle reflectance that is used to characterize thin reflective coatings. When radiation strikes thin coatings, the effects of internal reflection can cause the reflectance to vary according to the thickness of the coating.

Reflection is the ability of the surface of a material to reflect the solar radiation that impinges on it, modifying its direction or intensity. Many surfaces can be classified as specular (symmetrically modifies direction) or diffuse (reflection is distributed in a set of directions according to a geometric law called Lambertian). However, in reality, almost all surfaces have a mixture of both diffuse and specular reflectivity (see Fig. 05). Specular surfaces, such as glass, a water mirror or shiny metals, are those whose reflectivity is close to zero in all directions, except at the corresponding reflection angle. In contrast, diffuse surfaces, such as clothing, paper, asphalt and matt white paint, have equal (or almost equal) reflectivity values in all directions. The color of a surface directly influences the reflection factor of the surface (see Fig. 06).

Emissivity is the ability of the surface of a material to emit its own radiation as a result of its temperature. It is measured by the ratio between the intensity emitted by the surface of the evaluated material and the intensity that would be emitted by a blackbody at the same temperature and wavelength. The lower the emissivity value, the better the insulation of the surface by reflection, with 1 being the maximum value.

Specific outer coatings have been developed and applied to prevent solar radiation absorbed as heat by a surface from being transmitted to the interior by radiation or conduction. The American Society of Testing and Materials (ASTM) identified this property as “thermal emittance” and established a method for its measurement (ASTM C1371 Test Method for Determining the Emittance of Near-Room Materials Using Portable Emisometers). ASTM considers that a coating can be considered an Internal Radiation Control System (IRCCS) when it does not exceed the standard of 0.25.

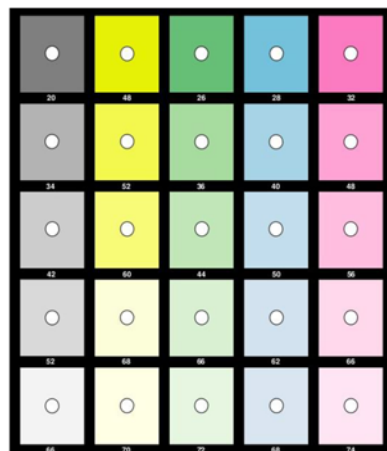
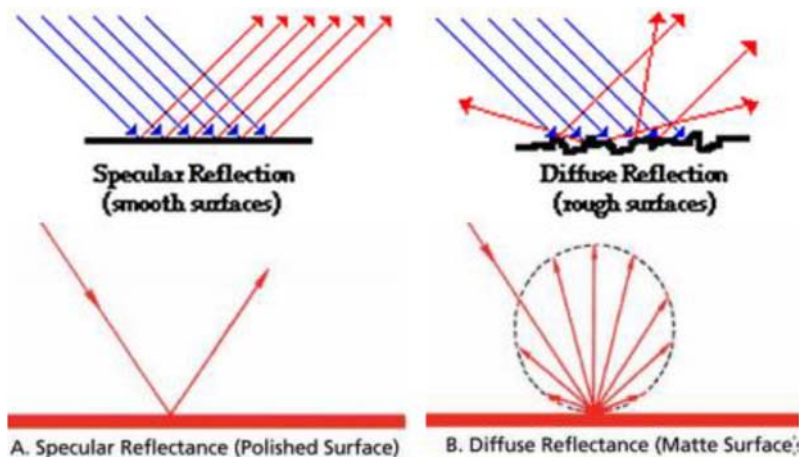


Figure 05. Specular and diffuse reflection

Source: <http://www.physicsclassroom.com/class/refln/Lesson-1/Specular-vs-Diffuse-Reflection>

Figure 06. Reflection factors of some colors

Source: J.A Taboada, *Manual del Alumbrado Osram*, Editorial Dossat

Therefore, from the perspective of thermal comfort, the suitability of a material for exterior cladding in architecture is determined by its reflectance and emissivity properties. At a practical level, the combined parameter is called the Solar Reflectance Index (SRI), which is an indirect measure of the ability of an opaque architectural exterior coating to reject solar heat from incident radiation. A scale ranging from standard black coating (reflectance 0.05 and emissivity 0.9) of value 0 to standard white coating (reflectance 0.8 and emissivity 0.9) of value 100 is defined for this purpose. For example, the temperature of standard black coating rises 50°C if exposed to full sun, while the temperature of standard white coating rises 8.1°C if exposed to full sun. Once the maximum temperature rise of a particular material has been determined for full sun, the SRI value can be calculated by interpolating between the values of 100 for the target and 0 for black. The SRI index is therefore a dimensionless scale from 0 to 100, where 0 is the most suitable value for absorbing and radiating heat (e.g. a tar coating) and 100 the value of the most reflective material, that is, the least heated (e.g. ice).

Radiative properties, temperature rise, and SRI of various building materials as reported in the LBNL Cool Roofing Materials Database.

Product	Solar Reflectance	Emissivity	Temperature Rise*	SRI
Clay tile, red	0.33	0.9	58	36
Concrete tile, red	0.18	0.91	71	17
Concrete tile, white	0.73	0.9	21	90
Asphalt shingles, white	0.21	0.91	68	21
Limestone pavers**	0.53	0.89	-30	62

*Maximum roof temperature rise.
 **Average of three light-colored, honed limestones reported from Valder's Stone & Marble, Inc., who used an accredited CRRC testing facility to evaluate their stone. Temperature Rise is predicted by UT based on the known linear relationship between this variable and SRI. This data is not reported by the LBNL.

Figure 07. Radiant characteristics, maximum temperature and SRI values for different types of urban pavements.

Source: The University of California's Lawrence Berkeley National Laboratory (LBNL), the leading research group on cool roofing materials, publishes a list of common building materials' SRI values. Table 1 displays some of these values.

Retrieved from: <http://www.naturalstonecouncil.org/content/file/Case%20Studies/Solar%20Reflectance%20Case%20Study%20-%2020071709.pdf>

1.4. Near-infrared pigments

In the construction sector, it is not easy to change existing exterior cladding materials for more efficient ones that can control the undesirable effects of incident solar radiation. It is more practical and feasible to pigment the most common coating materials (paints and plasters) with products that are highly selective to the near-infrared (NIR)

fraction of incident solar radiation, i.e. to increase reflectivity while reducing emissivity. Several authors and chemical companies [6, 7, 8, 9] are working to develop this type of additives for conventional opaque architectural coatings. In all cases, it is a question of combining cost, durability, efficiency and respect for the environment by developing new pigments that are complementary to light colors, such as white, which has already been shown to be reflective in the visible fraction (see Figure 8).

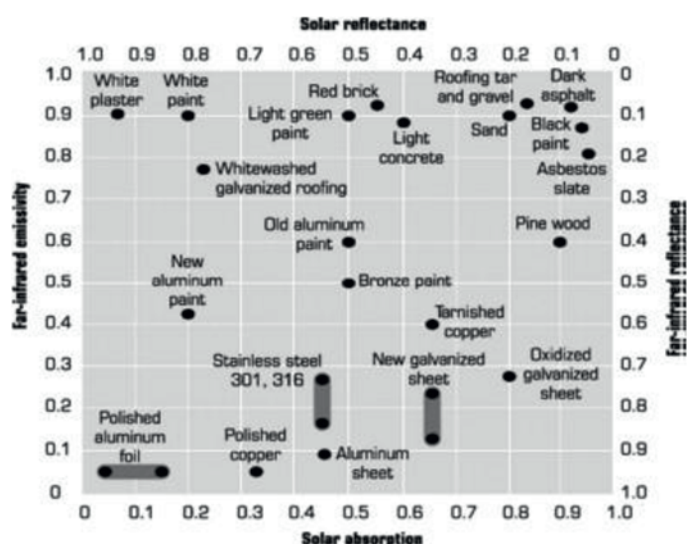


Figure 08. Spectral characteristics of building materials. Source: Florida Solar Energy Center (FSEC)

There have been developments in pigment for translucent materials such as mineral glass and some polymers. In the industry, some application systems have been developed that propose using a single direct, opaque reflecting layer. Other systems suggest the use of a previous layer of white color, which can prevent the absorption of heat energy transmitted by visible radiation, followed by a translucent layer with an NIR pigment selected to avoid absorption of heat energy transmitted by infrared radiation. Pigments of metallic origin can be used. Metals can be polished to make them shine so they have high reflectance, combined with low emissivity, which is why they are heated quickly and intensely by incident solar radiation (see Figure 07). In the case of low emissivity glass, metals, especially aluminum and silver, are pulverized to create thin layers of coatings, to increase reflectance and reduce emissivity. Two products that have been used for these purposes to date, due to their availability and attractive cost-benefit ratio, are:

- Titanium dioxide (TiO_2): the inorganic pigment with the highest reflectance. Due to its photocatalytic properties, it has been widely used in pigments as an air purifier, self-cleaner, and to promote the cooling of surfaces.
- Hollow glass microspheres: an attractive alternative because of their high mechanical strength, low density and production from pieces of recycled flat glass. In road signaling, the use of glass microspheres improves night vision, and is one of the most economical means to achieve this goal as the spheres reflect light in the direction from which it comes. The hollow structure gives the material appreciable characteristics of thermal insulation and near-infrared reflectance.

2. Hypothesis

In view of these data and available information, the aim of this study was to improve the thermal behavior of the exterior coatings that are usually used in social housing in the Dominican Republic. The proposed material was paint with added titanium dioxide and glass microspheres. We experimentally verified the behavior of different formulations of this coating and compared them to the behavior of conventional paint without NIR pigments. The study was supported by the Santo Domingo Technological Institute (INTEC), with the collaboration of Luis

Guillermo as technical advisor on equipment (see Figure 09) and Máximo Campusano, both from the Department of Energy Efficiency Laboratories.

3. Study

The experiment was carried out at the Residencial Franconia (Santo Domingo, Santo Domingo Este, at a latitude of 18° 29'14.20 "N and longitude of 69° 49'36.20" W) on an open-air platform located at a height of 2.60m. According to the data collected by the nearest meteorological station, the average annual temperature is 26.1°C, with a minimum of 19.9°C and a maximum of 31.8°C. For 26 consecutive days (20 December 2015–17 January 2016), the following were measured: incident solar radiation, temperature and relative humidity of the environment and surface temperature of the evaluated coatings on the surfaces of the following prototypes constructed for this purpose (see Figures 10–15):

- 2 prototypes representing the most common façades and roofs in social housing (V)
- 4 prototypes of facade walls, grouped into two (2) types (A and B),
- 2 deck prototypes, grouped into two (2) types (C and D)

The composition of the various blends of white acrylic paint with NIR pigments were as follows:

- White acrylic paint with 30% glass microspheres
- White acrylic paint with 30% glass microspheres and 20% TiO₂
- White acrylic paint with 50% glass microspheres
- White acrylic paint with 50% glass microspheres and 30% TiO₂

Measurements were taken daily on each of the main faces of the prototypes (east and west) from 10 am to 4pm, at 3-hour intervals. At all times, the incident solar radiation and the relative humidity of the environment each day were considered as important variables.



Instrument image	Name	Description
	Thermometer	Ebro Logger EBI 20
	Contact telethermometer	Center 309

Figure 09. Identification and characteristics of the measuring equipment

Type V: a real house was built in Santo Domingo, with a west-facing façade and roof both painted with white acrylic paint without NIR pigments. This house was used as a control to compare the measurements made on the surfaces of the façade and roof prototypes in which the same paint had been used, but with the addition of NIR pigments.

- V1 indicator: façade of concrete block masonry work + cement mortar coating + white paint
- V2 indicator: reinforced concrete roof + cement mortar coating + white paint

Type A: on the roof of V2 were built (4) walls of concrete block masonry work of 80 x 60 x 20 cm and portland cement mortar coating, facing west.

- Prototype A1: concreteblock masonry work wall + cement mortar coating + white paint with 30% glass microspheres
- Prototype A2: concreteblock masonry work wall + cement mortar coating + white paint with 30% glass microspheres and 20% TiO₂
- Prototype A3: concreteblock masonry work wall + cement mortar coating + white paint with 50% glass microspheres
- Prototype A4: concreteblock masonry work wall + cement mortar coating + white paint with 50% glass microspheres and 30% TiO₂

Type B: on the roof of V2 were built (4) walls of expanded polystyrene structural panels (EPSP) 80 x 60 x 20 cm and cement mortar coating facing west

- Prototype B1: expanded polystyrene panel wall + cement mortar coating + white paint with 30% glass microspheres
- Prototype B2: expanded polystyrene panel wall + cement mortar coating + white paint with 30% glass microspheres and 20% TiO₂
- Prototype B3: expanded polystyrene panel wall + cement mortar coating + white paint with 50% glass microspheres.
- Prototype B4: expanded polystyrene panel wall + cement mortar coating + white paint with 50% glass microspheres 30% TiO₂



Figure 10. Photographs taken during the prototyping process

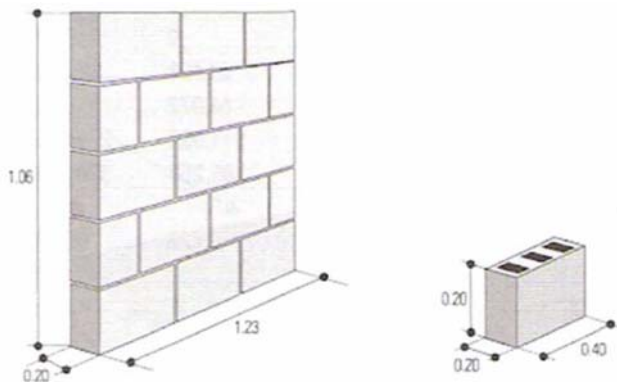


Figure 11. Type A: 80x60x20 cm prototype wall of concrete block masonry and portland cement mortar coating

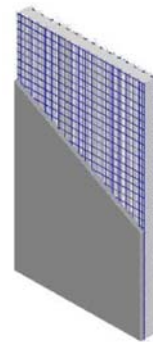


Figure 12. Type B: Prototype wall of 80x60x20 cm, composed of a nucleus of EPS of variable thickness between 4–28cm, an electro-welded steel mesh on both sides, and a cement mortar coating no less than 2.5 cm thick

Type C): (2) prototypes of bidirectional reinforced concrete roofs with a thickness of 12cm were built on roof V2 (see Figure 14)

- Prototype C1: reinforced concrete roof + white paint with 30% glass microspheres
- Prototype C2: reinforced concrete roof + white paint with 30% glass microspheres and 20% TiO₂
- Prototype C3: reinforced concrete roof + white paint with 50% glass microspheres
- Prototype C4: reinforced concrete roof + white paint with 50% glass microspheres and 30% TiO₂

Type D): (2) prototypes of polystyrene covers (EPS) with a thickness of 12cm were built on roof V2 (see Figure 15)

- Prototype D1: polystyrene cover (EPS) + white paint with 30% glass microspheres
- Prototype D2: polystyrene cover (EPS) + white paint with 30% glass microspheres and 20% TiO₂
- Prototype D3: polystyrene cover (EPS) + white paint with 50% glass microspheres
- Prototype D4: polystyrene cover (EPS) + white paint with 50% glass microspheres and 30% TiO₂



Figure 13. Photographs taken during the prototyping process

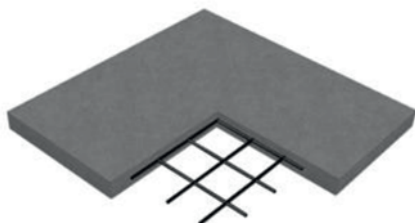


Figure 14. Axonometric view of the reinforced concrete bidirectional roof prototype with a thickness of 12cm. Retrieved from: <http://www.google.com.do/searchimages>

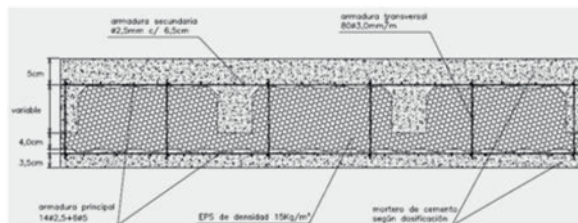


Figure 15. Sectional view of the prototype foam polystyrene foam (EPS) with a thickness of 12cm

4. Interpretation of results

Figure 16 shows the mean temperatures and the average relative humidity to which the experimental prototypes were subjected during the study period. The average daily percentage of humidity experienced during the study period was 74.9%. The average temperature was about 27°C, which is equivalent to the average annual temperature of the city of Santo Domingo, where the experiment took place. The value of the average horizontal solar radiation during the study period was 5.07 kWh/m²/d, according to NASA surface meteorology and solar energy data.

Figure 17 shows the graphs of the surface temperature records of west-facing walls at 4 pm for the prototypes of type A and B walls. Irregular behavior was observed as a consequence of climate variables (solar radiation, wind, humidity and temperature), but almost all prototypes were affected.

To facilitate the interpretation of the results at this preliminary stage, we focused on the day (23.12.2015) with the highest ambient temperatures (29.6°C) and analyzed the average temperature of each prototype during the 26 days of measurement.

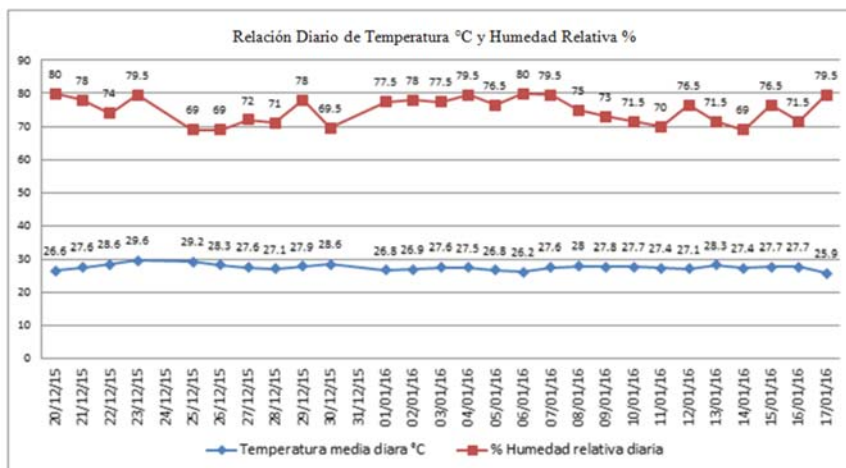


Figure 16. Graph of average daily measurements of ambient temperature and relative humidity during the study period

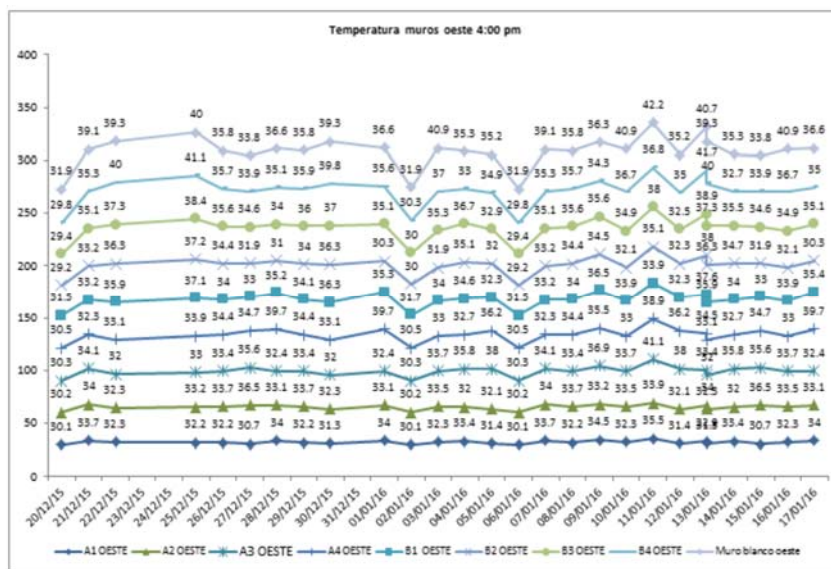


Figure 17. Record of temperatures on west-facing surfaces at 4pm in the prototypes of type A and B walls

Figure 18 shows the results of measuring the surface temperatures of west-facing walls during the 23 December 2015. The prototype A1 (30% glass microspheres) achieved the best performance (lower surface heating) relative to the wall with conventional white acrylic coating (V1). The order of decreasing efficiency of this series is as follows:

- A1 west, temperatures ranging from 32.8 to 32.9°C and an improvement of 6.70°C (1pm) to 7.80°C (4pm)
- A3 west, temperatures ranging from 34.9 to 33.4°C and an improvement of 4.60°C (1pm) and 7.30°C (4pm)
- A2 west, temperatures ranging from 34.5 to 34.0°C and an improvement of 5°C (1pm) and 6.70°C (4pm)
- A4 west, temperatures ranging from 36.9 to 34.5°C and an improvement of 2.6°C (1pm) and 6.20°C (4pm)

The levels of relative improvement in west-facing type B surfaces did not exceed those reached by type A surfaces. Throughout the day, the most inefficient surface was that of prototype B4, which even exceeded the surface temperature of the conventional wall (V1) by 1°C.

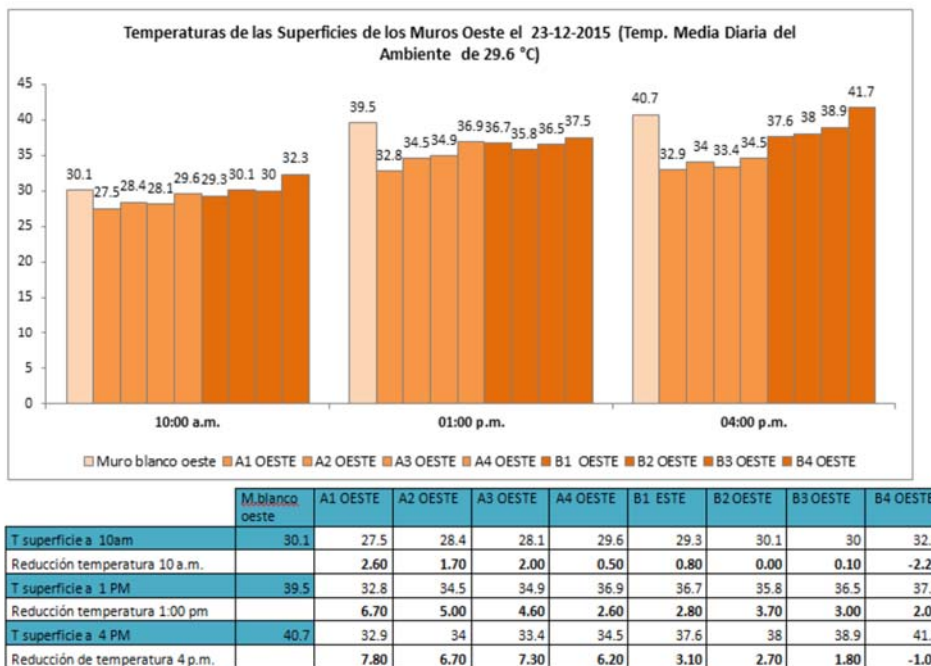


Figure 18. Graph of temperatures on the 23 December 2015 taken at three times and only for west-facing surfaces of experimental walls

Figure 19 shows the results of measuring surface temperatures of the east-facing walls during the 23 December 2015. Prototype A1 (30% glass microspheres) again showed the best behavior, with reductions up to 3.90°C (10am) and 4.40°C (1pm) relative to the white (V1) wall of conventional acrylic coating. The order of decreasing efficiency of this series in the morning is as follows:

- A1 East, with temperatures of 30°C and an improvement of 3.90°C during the morning (10am)
- A3 East, with temperatures of 31°C and an improvement of 2.90°C during the morning (10am)
- A4 East, with temperatures of 31.3°C and an improvement of 2.60°C during the morning (10am)
- A2 East, with temperatures of 32.5°C and an improvement of 1.40°C during the morning (10am)

The relative improvement in type B east-facing surfaces did not surpass that attained by surfaces of the A type walls during the morning. During this period, the most inefficient surface was that of prototype B3, which even surpassed the surface temperature of the conventional wall (V1) by 2.40°C. However, as the day progressed, towards 1 pm, the capacity of type B walls to reduce the temperature increased to equal that of type A walls. The order of decreasing efficiency of this series in the afternoon is as follows:

- A1 east, with temperatures of 32.4°C and an improvement of 4.40°C at 1pm
- B2 east, with temperatures of 33.0°C and an improvement of 3.80°C at 1pm
- B3 east, with temperatures of 33.2°C and an improvement of 3.60°C at 1pm
- B4 east, with temperatures of 34.2°C and an improvement of 2.60°C at 1pm

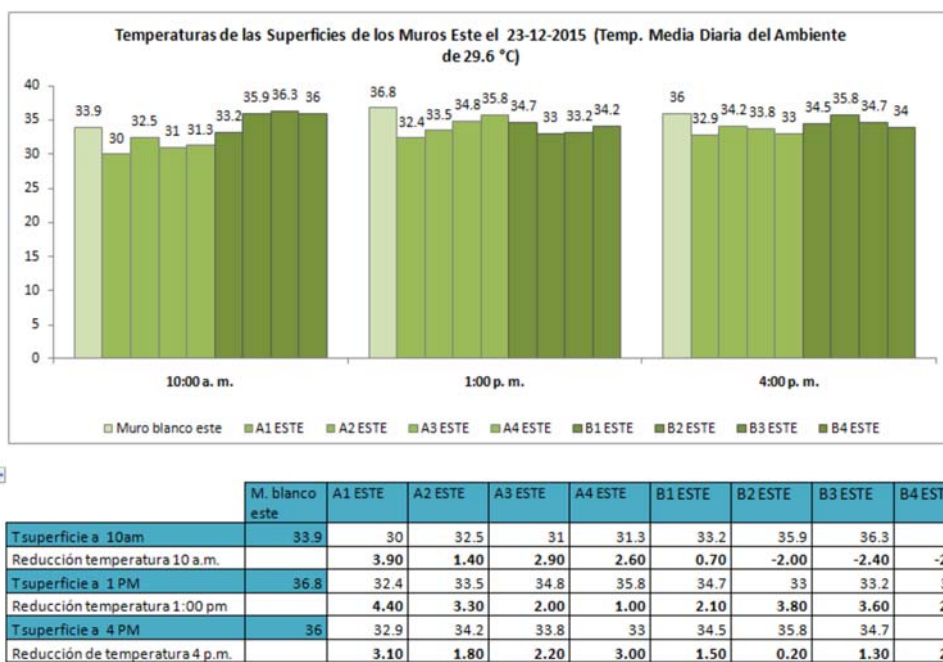


Figure 19. Graph of temperatures on 23 December 2015 taken at three times and only for east-facing surfaces of the experimental walls

Figure 20 shows the results of the surface temperature measurement for deck surfaces on 23 December 2015. The order of decreasing efficiency of this series in the morning is as follows:

- D1, with temperatures of 32.2°C and an improvement of 6°C during the morning (10am)
- C2, with temperatures of 32.5°C and an improvement of 5.70°C during the morning (10am)
- D3, with temperatures of 33.8°C and an improvement of 4.40°C during the morning (10am)
- D4, with temperatures of 34.3°C and an improvement of 3.90°C during the morning (10am)

The order of decreasing efficiency of this series at noon is as follows:

- C2, with temperatures of 33.6°C and an improvement of 7.9°C around midday (1pm)
- C1, with temperatures of 34.5°C and an improvement of 7.0°C around midday (1pm)
- D3, with temperatures of 34.5°C and an improvement of 7.0°C around midday (1pm)
- C3, with temperatures of 35.0°C and an improvement of 6.5°C around midday (1pm)

The order of efficiency of this series in the afternoon is as follows:

- D4, with temperatures of 32.6°C and an improvement of 10°C during the afternoon (4pm)
- C2, with temperatures of 32.9°C and an improvement of 9.7°C during the afternoon (4pm)
- D2, with temperatures of 33.4°C and an improvement of 9.2°C during the afternoon (4pm)
- D3, with temperatures of 33.6°C and an improvement of 9.0°C during the afternoon (4pm)

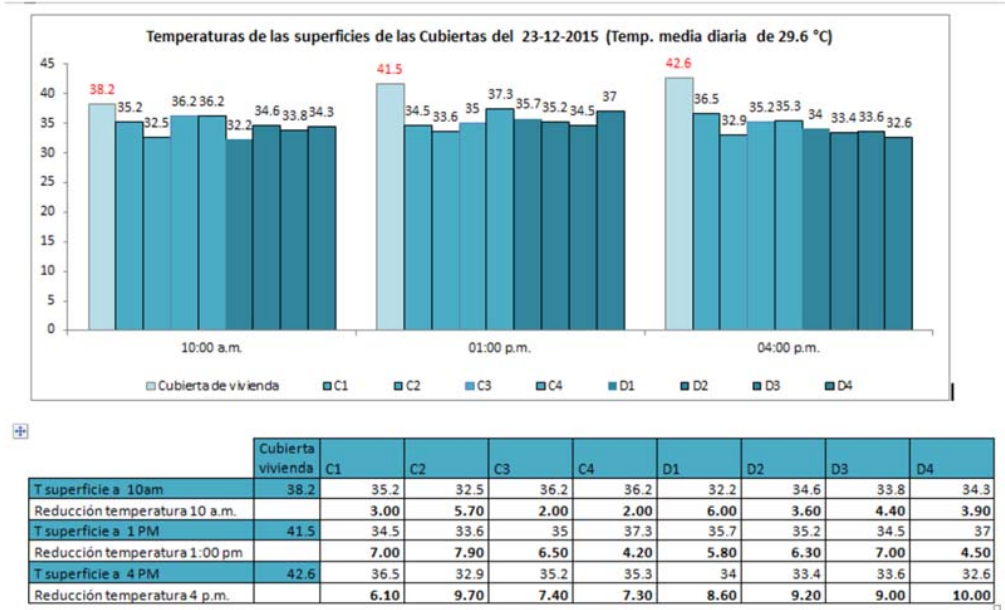


Figure 20. Graph of temperatures on 23 December 2015 taken at three times and for all the experimental surfaces of deck

We then repeated the previous analysis, but using the average data for all the days in the study period.

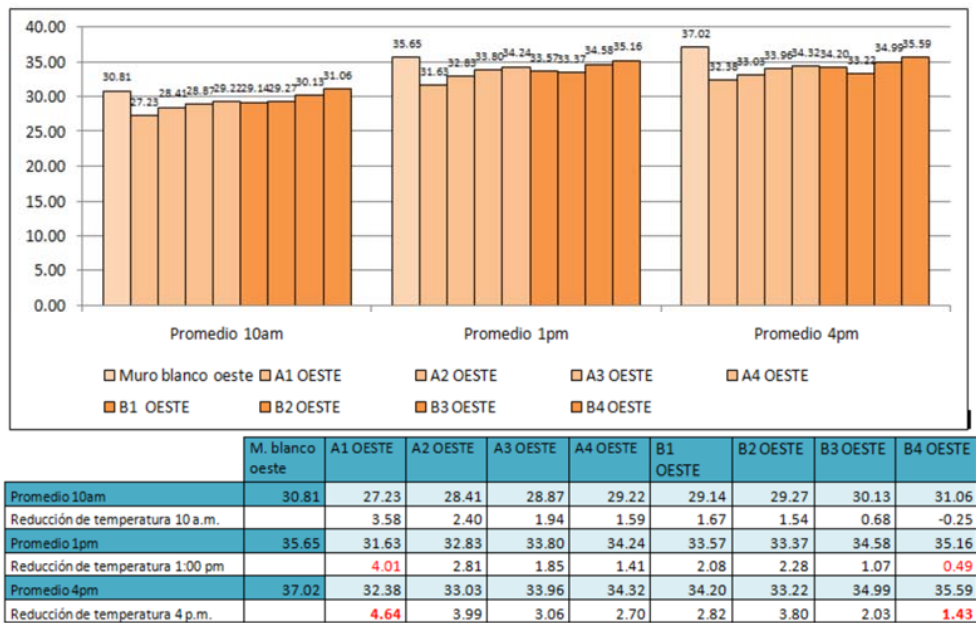
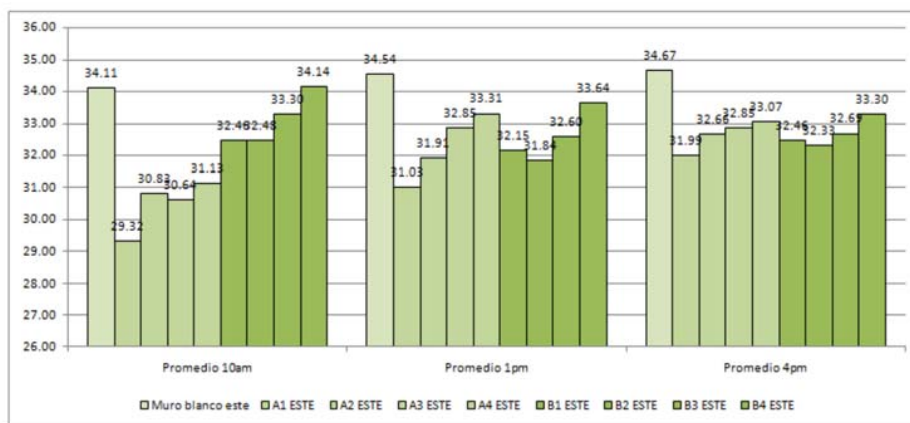


Figure 21. Graph of average temperatures taken three times per day, for west-facing wall prototypes

Figure 21 shows the average surface temperatures of west-facing walls for the entire experimental period. The prototype A1 (30% glass microspheres) again stood out as the best performing (least surface heating), compared to the white (V1) wall of conventional acrylic coating. The difference in average temperatures was maintained throughout the rest of the afternoon in all cases. The order of decreasing efficiency of this series is as follows:

- A1 west, average temperatures of 31.63°C (1pm) and 32.38°C (4pm), with improvements of 4.01°C (1pm) and 4.64°C (4pm) respectively.
- A2 west, average temperatures of 32.83 °C (1pm) and 33.03°C (4pm), with improvements of 2.81°C (1pm) and 3.99 °C (4pm) respectively.
- B2 west, average temperatures of 33.37°C (1pm) and 33.22°C (4pm), with improvements of 2.28°C (1pm) and 3.80°C (4pm) respectively.

Throughout the day, the most inefficient surface was again prototype B4. The temperature of this surface was closer to the surface temperature of the conventional wall (V1) by +0.25°C (10am) and -0.49°C (1pm). All prototypes showed some improvements, with the capacity to reduce temperatures increasing slightly throughout the day.



	M. blanco este	A1 ESTE	A2 ESTE	A3 ESTE	A4 ESTE	B1 ESTE	B2 ESTE	B3 ESTE	B4 ESTE
Promedio 10am	34.11	29.32	30.83	30.64	31.13	32.46	32.48	33.30	34.14
Reducción de temperatura 10 a.m.		4.79	3.29	3.47	2.98	1.66	1.63	0.82	-0.03
Promedio 1pm	34.54	31.03	31.91	32.85	33.31	32.15	31.84	32.60	33.64
Reducción de temperatura 1:00 pm		3.50	2.63	1.69	1.23	2.39	2.70	1.93	0.90
Promedio 4pm	34.67	31.99	32.66	32.85	33.07	32.46	32.33	32.69	33.30
Reducción de temperatura 4 p.m.		2.68	2.00	1.82	1.60	2.20	2.34	1.98	1.37

Figure 22. Graph of average temperatures, taken three times of day for the east side of the prototypes of walls

Figure 22 shows the average results of the measurement of surface temperatures on the walls only, taken on their east faces during the entire experimental period. Again, prototype A1 showed the best average behavior, with reductions of up to 4.79°C (10am) relative to the white wall (V1) of conventional acrylic coating. The order of efficiency of this series is as follows:

- A1 east, with temperatures of 29.32°C (10am) and an improvement of 4.79°C (10am) during the morning
- A2 east, with temperatures of 30.83°C (10am) and an improvement of 3.29°C (10am) during the morning
- A3 east, with temperatures of 30.64°C (10am) and an improvement of 3.47°C (10am) during the morning

However in the early afternoon (1pm) the most efficient surfaces were again prototypes A1, B2 and A2, with reductions of 3.50°C, 2.70°C and 2.63°C respectively. Throughout the day, the most inefficient surface was B4, whose temperature was closer to the conventional wall by +0.03°C (10am), although there was an improvement to -0.90°C at the beginning of the afternoon.

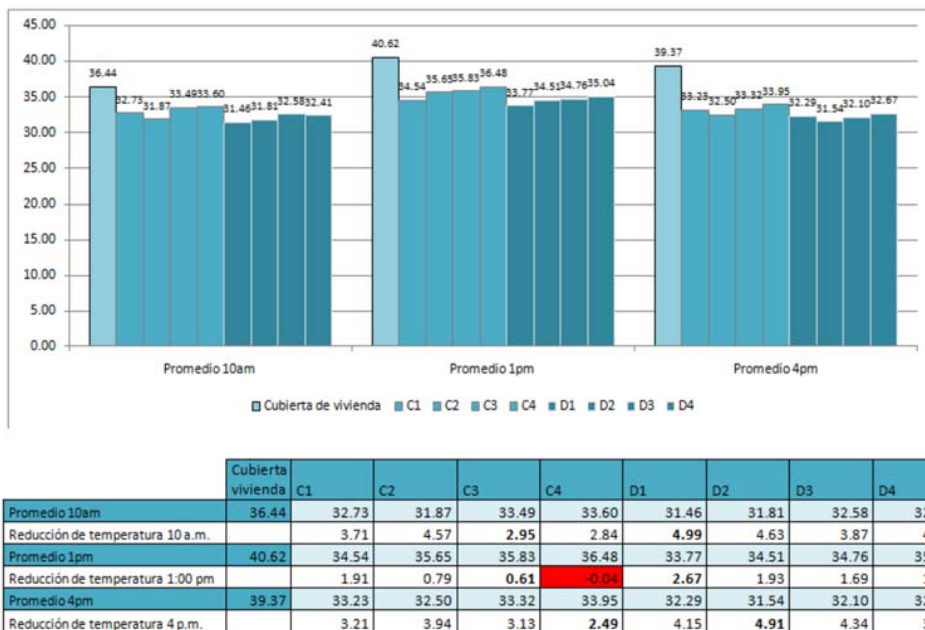


Figure 23. Graph of average temperatures taken at three times of day, for the face of the deck prototypes

Figure 23 shows the average results of measuring surface temperatures of the covering surfaces. Prototype D1 performed best relative to the conventional roof surface, with a difference of 4.99°C (10am) during the morning and 2.67°C in the early afternoon (1pm). In the afternoon, when the highest temperature levels were recorded, the most efficient cover surface was D2, with a difference of 4.91°C. Throughout the day, the type D covers were cooler than those of type C, in a general sense. However, the C1 surface also experienced a reduction of up to 4.57°C (10am). The order of decreasing efficiency of this series in the morning is as follows:

- D1, with temperatures of 31.46°C and an improvement of 4.99°C during the morning.
- D2, with temperatures of 31.81°C and an improvement of 4.63°C during the morning.
- C2, with temperatures of 31.87°C and an improvement of 4.57°C during the morning.

Throughout the day, the most inefficient surface was C4. The temperature of C4 was higher than that of the conventional deck by +0.04°C at 4pm, but reduced during the morning-afternoon by -2.84°C and -2.49°C respectively.

5. Conclusions

- The values obtained after the preliminary experiment with NIR pigments incorporated in conventional white acrylic paint covering vertical walls of social housing in the Dominican Republic showed that the most effective solution was prototype A1: concrete factory wall + cement + white acrylic paint with 30% glass microspheres. The average reductions in temperatures using this prototype were 4.79°C to the east and 4.64°C to the west, with a maximum reduction during the hottest day of 4.40°C to the east and 7.80°C to the west.
- Although type A (concrete block masonry) walls registered on average greater reductions in temperature and efficiency than type B walls (with an EPS core), as the hours of the day advanced and the surface became warmer, B walls also increased their capacity to reduce temperature. This may be due to the fact that the concrete block system has lower thermal resistance, with a thermal delay of 2 hours, while polystyrene has a delay of 8 hours.
- The values obtained after the preliminary experiment with NIR pigments incorporated in conventional white acrylic paint covering roofs of social housing in the Dominican Republic revealed that the most effective solution

was prototype D1: polystyrene cover (EPS) + white paint with 30% glass microspheres, with an average reduction in temperature of 4.99°C.

- It is noteworthy that 30% of glass microspheres were more efficient in the experimental set, whereas paint with TiO₂, only contributed significantly to the increase in reflectance in the specific cases of covers.
- Generally speaking, all the coatings were efficient to some extent, although some less than others. This shows that the use of glass microspheres as an addition in paints improves the reflectance indices of the surfaces by reducing the effects of heat by radiation.

Acknowledgements

This paper is a part of a final project carried out for the master's degree in Technology of Architecture at the *Universitat Politècnica de Catalunya* (UPC) in the 2015–2016 academic years. The Spanish version can be consulted at: <https://upcommons.link.upc.edu/handle/2117/89334>

References

- [1] Banco Nacional de Fomento de la Vivienda y la Producción (BNV), April 2015. Retrieved from: <http://www.bnv.com.do/>
- [2] Caminero, H. *Incidencia térmica y lumínica de los pavimentos exteriores en el exterior de la vivienda para clima cálido-húmedo caso Santo Domingo, República Dominicana*. Barcelona 2012: Universidad Politècnica de Catalunya. Retrieved from: <https://mastersuniversitaris.upc.edu/aem/archivos/2011-2012-tesinas-pres/03-HypatiaCaminero->
- [3] Fundación Global. *Clima de Republica Dominicana*. Retrieved from: http://www.dominicanaonline.org/portal/espanol/cpo_clima3.asp
- [4] Bryan Urban and Kurt Roth, P. (2010). *Guidelines for Selecting Cool Roofs*. Retrieved July 2015 from: Fraunhofer Center for Sustainable Energy Systems, U.S. Department of Energy Building Technologies Program and Oak Ridge National Laboratory. https://heatland.lbl.gov/sites/all/files/coolroofguide_0.pdf
- [5] Doulos L., S. M. (2004). *Passive cooling oh the OutdoorUrban Spaces- the Role of the Materials*. Sol. Energy, 77(2), 231-249.
- [6] Reza, K. B. (2015). *Pavement made of concrete with highsolar reflectance*. (p. 37). Minnesota, USA.
- [7] Fernando Pacheco-Torgal, J. L. (2015). *Eco-efficientMaterials for Mitigating Building Cooling Needs: Design, Properties and Application*. Woodhead Publishing Series in Civil and Structural Engineering.
- [8] José, S. R. (2013). *Lanthanum-stronium copper silicates asintense blue inorganic pigments with high near-infraredreflectance*. Dyes Pigm, 98(3), 540-546.
- [9] Kinouchi T., Y. T. (2003). *Development of cool pavementwith dark colored high albedo coating*. Target, 50(40).
- [10] Levinson, R. A. (2001). *Effects on composition and exposure on the solar reflectance of Portland Cement Concrete*. Cement and Concrete Research, 32(11).
- [11] Medgar L. Marceau, M. G. (2008). *Solar Reflectance Values of Concrete*. Concrete International, 30(8).
- [12] RIMA (2003) *Reflective Insulation, Radiant Barriers and Radiation Control Coatings*. Reflective Insulation Manufacturers Association International (RIMA-I) Retrieved from: <http://www.rimainternational.org/pdf/handbook.pdf>
- [13] Uemoto K. L., S. N. (2010). *Estimating thermal performance of cool colored paints*. Energy and Buildings, Volume 42, Issue 1, January 2010, Pages 17–22, International Conference on Building Energy and Environment (COBEE 2008)
- [14] Wan W. C., Hien, W. N., Ping T. P. , Aloysious A. Z.(2012). *A study on the effectiveness of heat mitigating pavement coatings in Singapore*. Journal of Heat Island Institute International, Vol.7-2 (2012)
- [15] Wang, J. L. (2013). *Synthesis and Characterization of NiTiO₃ yellow nano pigment with high solar reflection efficiency*. Powder Technology (235) Elsevier.
- [16] Muntané, O. (2012) *Espill: “re-roofing the cities”: prevenir el canvi climatic*. Retrieved from: <http://upcommons.upc.edu/handle/2099.1/14134>